CHAPTER X

SYNTHESIS AND LUMINESCENCE PROPERTIES OF ZNS AND METAL (MN, CU)-DOPED-ZNS CERAMIC POWDER

10.1 Abstract

ZnS and metal (Mn, Cu)-doped-ZnS were successfully prepared by wet chemical synthetic route. The understanding of substituted metal ions (Mn, Cu) into ZnS leads to transfer the luminescent centre by small amount of metal dopant (Mn, Cu). Fourier transform infrared and X-ray diffraction were used to determine chemical bonding and crystal structure, respectively. It showed that small amount of metal (Mn, Cu) can be completely substituted into ZnS lattice. X-ray fluorescence was used to confirm the existence of metal-doped ZnS. Scanning electron microscope revealed that their particles exhibits blocky particle with irregular sharp. Laser confocal microscope and photoluminescence spectroscopy showed that ZnS and metal-doped-ZnS exhibited intense, stable, and tunable emission covering the blue to red end of the visible spectrum. ZnS, Mn-doped-ZnS and Cu-doped-ZnS generated blue, yellow and green color, respectively.

10.2 Introduction

As a wide band-gap semiconductor with a range of band-gap energy of 3.6-3.9 eV, ZnS has been widely applied to make numerous optical devices such as ultraviolet light-emitting diodes [214-216] , flat panel display [2] and thin film electroluminescence [217-219]. Various ZnS crystal structures including bulk and nano-particle such as sphere, rod, tube and wire have been successfully synthesized by using diverse methods and their luminescent properties have been investigated [53, 220, 221]. In recent years, accordingly, Mn-doped, Cu-doped and Mn-Cu-codoped ZnS powders have received much attention in research because many functions can be added by transporting and controlling numerous types of spin state. In addition, it can be indicated that the properties are closely related to the

concentration of metal-doped because it can change the energy band and form luminescence of different energy level.

Many approaches have been used for the preparation of pure ZnS and metal-doped ZnS and controlling their morphology has been reported. In 2001, Jiang et al have exhibited the in situ formation method for ZnS nanowires in the liquid crystal template [222]. In 2005, Charinpanitkul has synthesized ZnS nanoparticles in microemulsion and investigated the effect of surfactant on particle size [223]. In 2009, Li et al and Salavati-Niasari et al have prepared ZnS via layer-by-layer self-assembly technique [224] and hydrothermal synthesis [225], respectively. Recently, in 2010, Uekawa et al also found that ZnS nanoparticles can be successfully prepared by heating the mixture of ZnS precipitate and ethylene glycol [226]. However, these synthetic methods are relatively more complicated. The high reaction temperature in operation process and the use of organic solvent should be preferably avoided. In addition, the fluorescence intensity is far below the minimum requirement of optical devices at room temperature. The development of novel and simple synthetic route has therefore considered in order to obtain high yield of product.

In this research work, we wish to present the synthesis of ZnS and metal-doped ZnS ceramic powder by conventional and facile synthetic route using zinc sulfate and sodium sulfide as reagent materials. Metal ions induce impurity level by substituting the position of Zn^{2+} in the lattice of ZnS and consequently change the optical properties. The colorful fluorescence lights were consequently observed.

10.3 Experimental

10.3.1 Chemical Reagents

Sodium sulphide ($Na_2S. 9H_2O$) was purchased from Caledon Chemical Company, Canada. Zinc sulfate ($ZnSO_4. 7H_2O$), Cuprous chloride (CuCl) and Manganese sulfate ($MnSO_4. H_2O$) were purchased from J. T. Baker Chemical Company, Canada. Analytical grade of methanol was purchased from Bioshop, Canada. Distilled water and analytical grade of methanol were used as solvent. All the chemical reagents were used as received.

10.3.2 Instruments

- Fourier transform infrared spectroscopy (FTIR)

FTIR was performed on a Bruker Vector 22 mid-IR spectroscopy (Bruker, Germany), All FTIR absorption spectra were recorded over 4500-500 cm^{-1} wavenumbers region at a resolution of 8 cm^{-1} with 1024 scans using a deuterated triglycine sulfate (DTGS) detector. A straight line between two lowest points in the respective spectra region was chosen as a baseline. Potassium bromide (KBr) acting as a non-absorbing medium was mixed with a solid sample (0.3-0.5 wt %) by an agate mortar and pestle to prepare a pellet specimen.

- X-ray Diffraction (XRD)

The synthesized ceramic powders were stored in an oven above 150°C overnight for water absorption prevention. The crystal structure of the powders was analyzed by XRD (Phillips P.W. 1830 diffractometer) using nickel-filtered CuKα radiation. Diffraction patterns were recorded over a range of 25-80°. The consistency result was compared with literature [226].

- Scanning electron microscope (SEM) and energy dispersive analysis (EDX)

The powders were investigated by SEM (a JOEL JSM-6301F scanning microscope). The machine was operated at an acceleration voltage of 20 keV at a working distance of 15 mm to identify the morphological properties of powders. Before investigation, the samples were sputter-coated with Au to enhance the electrical conductivity.

- X-ray fluorescence (XRF)

XRF (A Phillips 1404 XRF Wavelength Disperse Spectrometer) was used to determine the trace element of sample. It equipped with an array of five analyzing crystals and fitted with a Rh X-ray tube target was used. A vacuum was used as the medium of analyses to avoid interaction of X-rays with air particle. 1 g of sample was mixed with 6 g of H_3BO_3 and consequently pressed under 10 tons of force.

- Laser confocal microscope and photoluminescence spectroscopy

Laser confocal microscope and luminescence experiments were performed using an Olympus BX41 fibre-coupled confocal microscope. Excitation of the dopant ions is performed using a continuous argon laser. The excitation beam was focused

on the sample surface by means of an 100 achromatic microscope objective (NA0.9) down to approximately 0.3 mm spotsize. To separate the excitation beam and the sample luminescence, an interferential filter that removes the excitation wavelength (notch filter) was used. The fluorescence was focused into a fibre-coupled high-resolution spectrometer (SPEX500M) and then detected using a CCD camera.

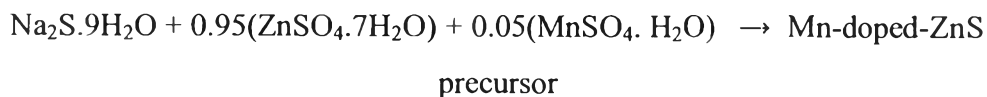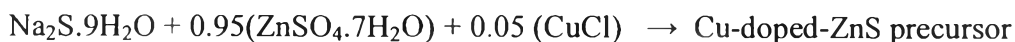- Preparation of ZnS and metal-doped ZnS powder

The ZnS ceramic powder was prepared as follow: 10 g of $Na_2S. 9H_2O$ was added to 50 ml of distilled water. The mixture was stirred for 1 hour. In parallel, 10 g of $ZnSO_4. 7H_2O$ was also dissolved into 50 ml of distilled water. $Na_2S. 9H_2O$ solution was then poured into $ZnSO_4. 7H_2O$ solution.

The stoichiometric of chemical reaction was below;

$$Na_2S.9H_2O + ZnSO_4.7H_2O \rightarrow ZnS \text{ precursor}$$

For the individual Mn-doped and Cu-doped ZnS ceramic powder, it was prepared as follow: 10 g of $Na_2S. 9H_2O$ was added to 50 ml of distilled water. The mixture was stirred for 1 hour. In parallel, 9.5 g of $ZnSO_4. 7H_2O$ and each of 0.5 g of CuCl and $MnSO_4. H_2O$ was also dissolved into 50 ml of distilled water. $Na_2S. 9H_2O$ solution was then poured into $ZnSO_4. 7H_2O$ solution.

The stoichiometric of chemical reaction was below;

$$Na_2S.9H_2O + 0.95(ZnSO_4.7H_2O) + 0.05 (CuCl) \rightarrow \text{Cu-doped-ZnS precursor}$$

$$Na_2S.9H_2O + 0.95(ZnSO_4.7H_2O) + 0.05(MnSO_4. H_2O) \rightarrow \text{Mn-doped-ZnS precursor}$$

On the other hand, for the co-metal doped ceramic powder, it was prepared as follow: 10 g of $Na_2S. 9H_2O$ was added to 50 ml of distilled water. The mixture was stirred for 1 hour. In parallel, 9 g of $ZnSO_4. 7H_2O$ and each 0.5 g of CuCl and $MnSO_4. H_2O$ was also dissolved into 50 ml of distilled water. $Na_2S. 9H_2O$ solution was then poured into $ZnSO_4. 7H_2O$ solution.
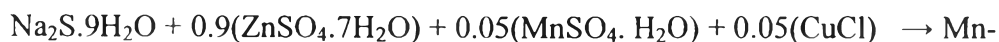
$$Na_2S.9H_2O + 0.9(ZnSO_4.7H_2O) + 0.05(MnSO_4. H_2O) + 0.05(CuCl) \rightarrow \text{Mn-Cu-codoped-ZnS precursor}$$

The reaction was continually conducted for 4 hours at room temperature. After the reaction was completed, methanol was employed to use in order to remove impurities, 50 ml of methanol was added and then the mixture was centrifuged at 500

rpm for 30 min. The obtained ZnS and metal-doped ZnS would precipitate. The step of adding methanol was repeated ten times and each of methanols was removed. The mixture was kept in oven at 150°C overnight.

10.4 Results And Discussion

- Fourier transform infrared spectroscopy (FTIR)

FTIR spectra of ZnS and ZnS doped with Cu and Mn are showed in Figure 9.1. The characteristic ZnS vibration peaks can be observed at 1120, 617, and 464 cm^{-1}. The peaks at 2924, 2850, 2364 and 1624 cm^{-1} are due to microstructure formation of the samples. The obtained peak values are in good agreement with the literatures [227, 228]. The broad absorption peak in the range of 3000-3600 cm^{-1} corresponding to –OH group indicates the existence of water absorbed in the surface of nanocrystals. The bands at 1500-1650 cm^{-1} are due to the C=O stretching modes arising from the absorption of atmospheric CO_2 on the surface of the nanocrystals [229].

The FTIR spectrum of ZnS doped with Mn shows similar peaks as the spectrum of pure ZnS particle. The peak at 1120 cm^{-1} split into two peaks, i.e. at 1120 and 1130 cm^{-1}, indicating that the doped Mn affected the structure of portion of the ZnS particles. In parallel, Cu doping had also an effect on the structure of ZnS. The peak at 1120 cm^{-1} split into two peaks, i.e. at 1120 and 1110 cm^{-1}, respectively. It can be explained that either Mn or Cu atom can be partially substituted into Zn position in ZnS crystal. In addition, it can be observed that Mn and Cu- codoped were successfully carried out. The peak at 1120 cm^{-1} split into three peaks, i.e. at 1110, 1120 and 1130 cm^{-1}, suggesting that both Mn and Cu atom were successfully substituted into main ZnS crystal. The appearing peaks at 1110 and 1130 were corresponded Zn-S-Mn and Zn-S-Cu, respectively. The partial metal substitution result was consistent with XRD experiment.
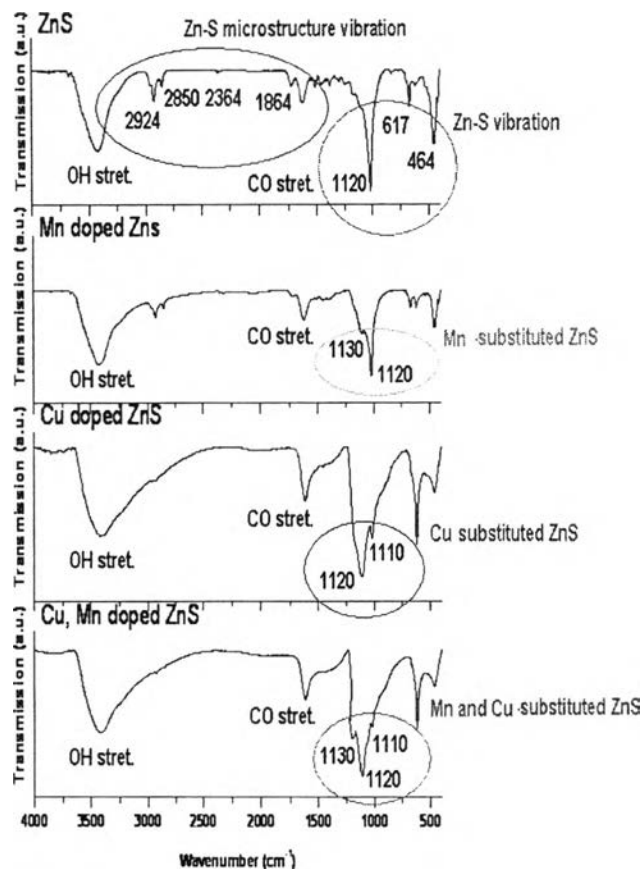
Figure 10.1 FTIR spectra of ZnS, and Mn doped ZnS, Cu doped ZnS and Mn-Cu codoped ZnS

- X-ray diffraction (XRD)

XRD pattern of ZnS and ZnS doped with Cu and Mn are showed in Figure 10.2. Three well-defined diffraction peaks corresponding to the lattice planes of (111), (220) and (311) can be observed in all samples. These peaks matched very well with the cubic zinc blended structure (JCPDS No. 05-0566), confirming the purity of the synthesized ZnS. As ZnS was doped with Mn and Cu, the (111) peak became broadened in all cases, along with the smaller relative intensity of peak (111) (Table 10.1), suggesting that the crystallinity of ZnS was degraded as a result of doping. Because of the size effect, XRD peaks broaden as the particle become smaller [142].

However, in the case of Cu doped samples, the XRD patterns showed additional peaks at 32°. The incomplete substitution occurred during experimental

reaction step. Partial amount of copper can not be well substituted due to non-sufficient energy.

Broadening of peaks indicates the nanocrystalline nature of the sample from XRD patterns. According to Debye-Scherrer formula, crystallite size can be calculated by this equation below,

$$D = k\lambda/(\beta\cos\theta)$$

Where D is the mean grain size, k is constant (shape factor, approximately 1), λ is the X-ray wavelength (1.54056 A° for Cu-Kα), β is the full width at half maximum (FWHM) of the diffraction peak and θ is the Bragg angle.

According to the FWHM of the most intense peak (111) plane, the average crystallite sizes of ZnS and metal-doped ZnS were showed in Table 10.1. The crystallite size of ZnS was 30 Å, but slightly dropped to the range of 22-28 Å as it was doped with Mn and Cu. The lattice parameter of ZnS also decreased. This is due to very small amount of impurity, and these ions were doped into ZnS lattice.
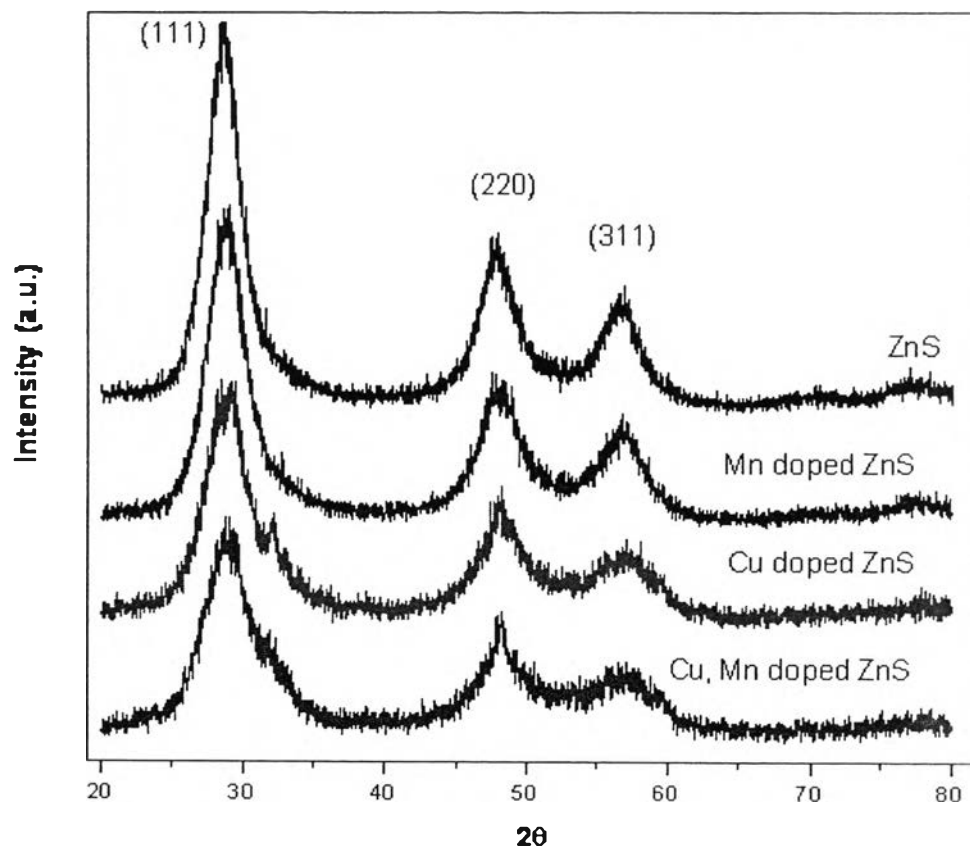
Figure 10.2 XRD pattern of ZnS, and metal (Mn, Cu)-doped-ZnS.

Table 10.1 Crystallite size and lattice parameter of ZnS, and ZnS doped with Cu and Mn.

Sample	Relative Intensity of Peak (111)	Crystallite Size, Å	Lattice Parameter, Å
ZnS	100	30	10.77
5%wt Mn-doped ZnS	78.6	28	10.75
5%wt Cu-doped ZnS	58.2	25	10.72
2.5%wt Cu-2.5%wt Mn-codoped-ZnS	49.2	22	10.69

- Scanning electron microscope (SEM) and energy dispersion analysis (EDX)
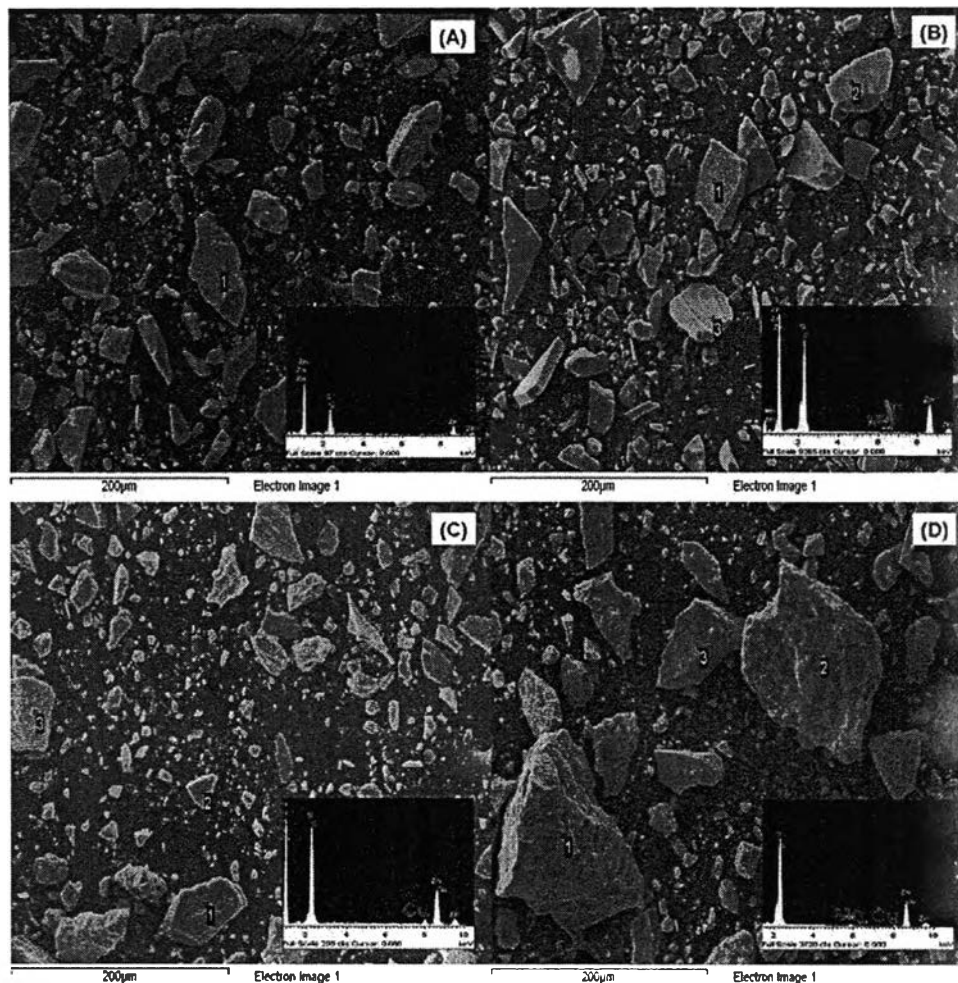

Figure 10.3 Field emission scanning electron microscope (FESEM) and energy dispersion analysis (A) ZnS (B) Mn-doped-ZnS (C) Cu-doped-ZnS (D) Mn-Cu-codoped-ZnS

Figure 10.3 exhibits the typical microstructure FESEM image of as-synthesized undoped ZnS and metal-doped ZnS. The powders exhibited blocky particles with irregular shapes possibly due to the agglomeration among particle. Therefore, the actual size of the nanoparticle can not be determined from the FESEM images as it is limited by its agglomeration and the resolution of the used FESEM instrument.

On the other hand, an X-ray energy dispersive spectroscopy (EDX) spectrum (the inset in Figure 10.3) acquired from the metal-doped ZnS confirm that the particles consist of Zn, S and related metal-dope (Mn and Cu) with mainly a

stoichiometric ZnS composition. The successive substitution of Mn and Cu-doped into ZnS cubic structure was successfully prepared. The amount of Mn and Cu atom was indicated on EDX spectrum which is consistent with added-amount in preparation step.

- X-ray Fluorescence (XRF)

XRF was used to determine the quantitative analysis of all samples. Table 10.2 represents the element contents of ZnS and metal-doped ZnS ceramic. The major elements of all samples are Zn and S, while the minor elements are Mn and Cu. In case of Mn-doped ZnS and Cu-doped ZnS, the existence of Mn and Cu is 3.141% and 6.481 %, respectively. However, in case of Mn-Cu-codoped ZnS, the existence of Mn and Cu is 7.904% and 2.330%. This result can confirm the presence of Mn-doped ZnS, Cu-doped ZnS and Mn-Cu-codoped ZnS. This analysis method is accurate with an experimental error of 10%. This is due to the counting statistic during measurement.

Table 10.2 XRF quantitative analysis of ZnS and metal-doped ZnS ceramic

Sample	Zn	S	Mn	Cu
ZnS	57.488	45.512	-	-
5%wt Mn-doped ZnS	60.110	39.577	3.141	-
5%wt Cu-doped ZnS	33.622	59.897	-	6.481
2.5%wt Cu-2.5%wt Mn-codoped-ZnS	33.823	55.943	7.904	2.330

- Photoluminescent characterization

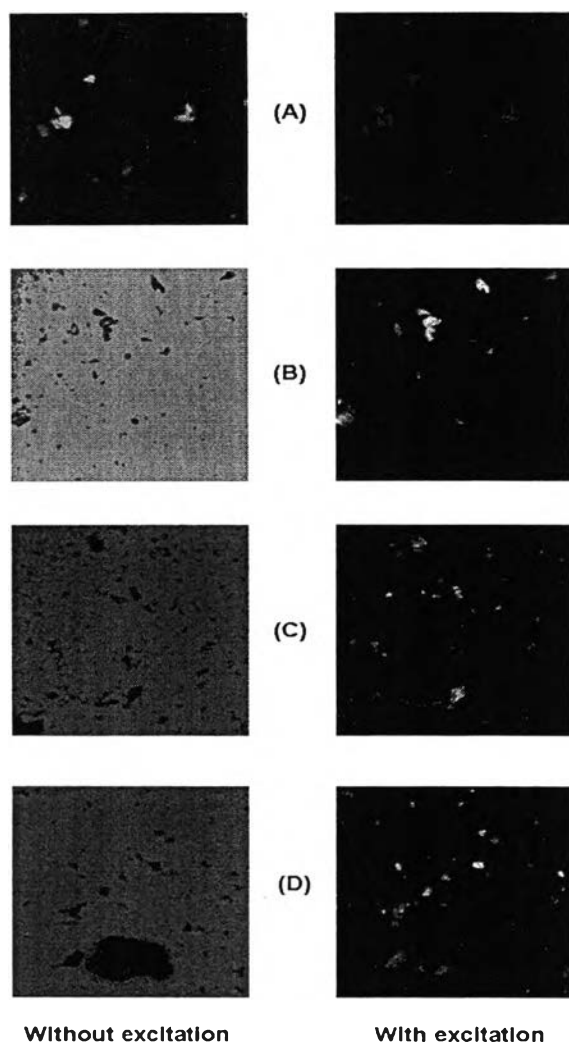Without excitation   With excitation

Figure 10.4 The fluorescence image of ZnS particle without excitation and the fluorescence image of ZnS particle with excitation (A) ZnS (B) Mn-doped-ZnS (C) Cu-doped-ZnS (D) Mn-Cu-codoped-ZnS

The fluorescence and room temperature photoluminescence (PL) spectra of ZnS and metal-doped ZnS are illustrated in Figure 10.4 and Figure 10.5, respectively.

ZnS particle and metal-doped ZnS particles were respectively dispersed on clean glass slides for fluorescence microscope observation. On the left hand side of

Figure 10.4, it shows a fluorescence image of ZnS and metal-doped ZnS particle without excitation, where various ZnS and metal-doped ZnS clusters were aggregated by small nanoparticles. In case of pure ZnS particle (A), under a UV light of 320 nm excited, the ZnS particles emit strong blue fluorescence light (Right hand side). The photoluminescence spectrum in Figure 10.5A exhibits a sharp PL at 450 nm, completely coinciding with the blue fluorescence light.

On the other hand, for the Mn-doped ZnS, a super-bright yellow with bluish fluorescence was observed when excited with 450 nm wavelength. In parallel, for the Cu-doped ZnS, a super-bright green fluorescence was observed at similar excitation as previous experiment. It exhibited a sharp strong PL band located at 595 and 517 nm, respectively. It can be noted that the strong yellow and green fluorescence are attributed to the transition emission from manganese and copper atom introduced energy level. Thus, metal-doped ions, as optically active luminescence centers, efficiently created the luminescence of particle. After metal-doped step, the luminescent centers were transferred to impurity ions.

For the Mn-Cu codoped ZnS, Mn^{2+} and Cu^{+} were then substituted into Zn^{2+} sites. The transition metallic ions have different d-d transitions, which result in the emission yellow. However, due to starting chemical reagents, Mn^{2+} and Cu^{+} were derived from $MnSO_4 \cdot H_2O$ and $CuCl$, respectively, suggesting that the matching oxidation number between Mn^{2+} and Zn^{2+}. Mn is more completely substituted in Zn position than Cu atom. However, in this Mn-Cu codoped ZnS, Cu was also used as substituted metal. It is controversial that XRF and EDX qualitative analysis exhibited Cu atom. Due to mismatching oxidation number of Cu and Zn, Cu can not be well substituted into ZnS crystal and may exist as other impurity (not Mn-Cu-codoped ZnS). The green color can not be detected.

On the other hand, the PL band located at 457 and 595 nm, showing both blue and yellow region, suggesting that partially substitution of Mn atom into ZnS. The sample may contain Mn-Cu-codoped ZnS and neat ZnS. It can be explained that Cu atom may affect this co-dope substitution step. Consequently, the substitution ability of Mn in Mn-Cu-codoped ZnS may be decreased from Mn-doped ZnS. However, this issue will be discussed later on.
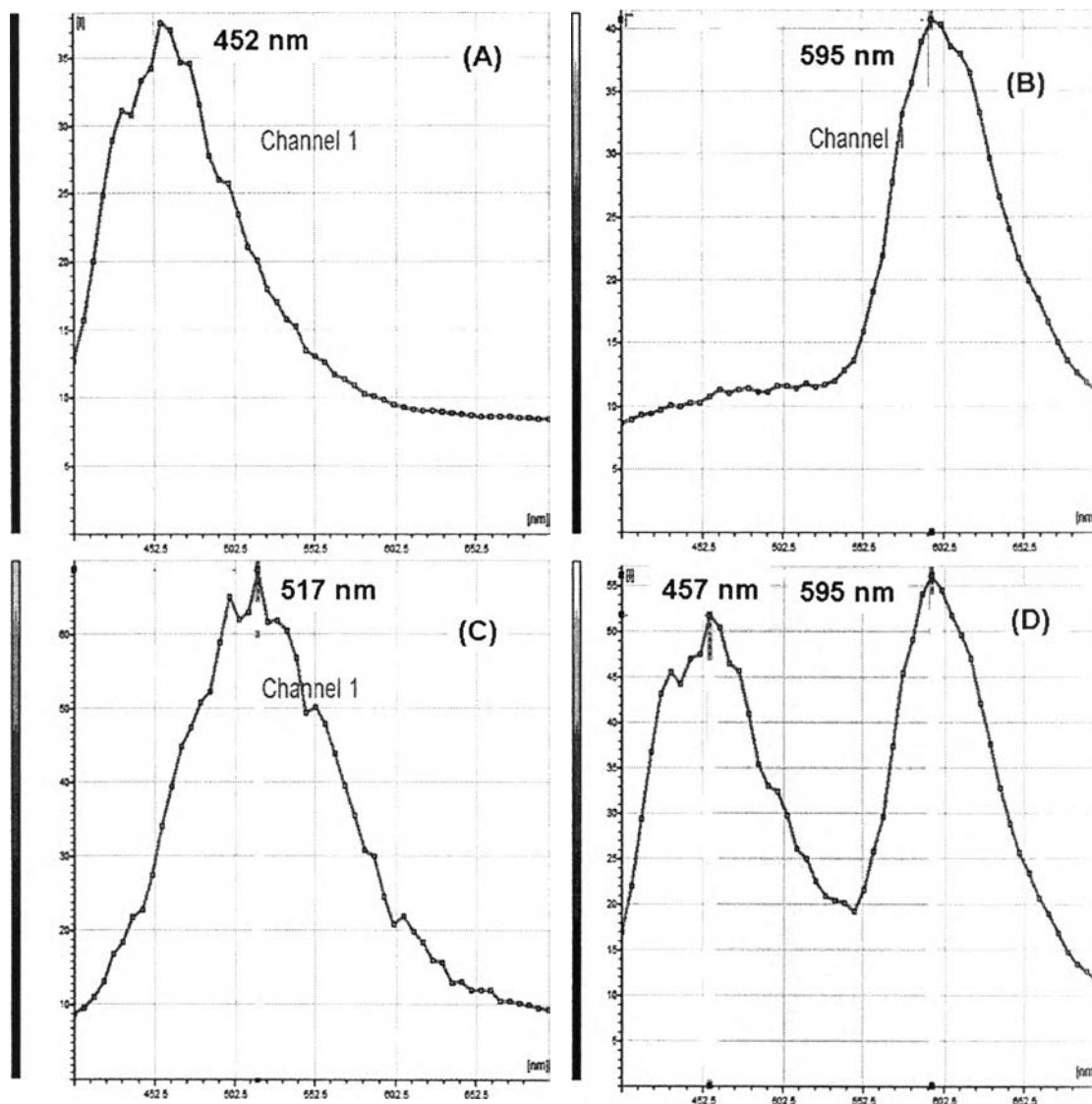
Figure 10.5 Photoluminescence spectra of ZnS and metal-doped ZnS particle
(A) ZnS (B) Mn-doped-ZnS (C) Cu-doped-ZnS (D) Mn-Cu-codoped-ZnS

On the other hand, in theory, it is well-known that metal-doped ZnS can be considered as a p-type semiconductor [230]. Mn and Cu state related emission is always expected at a lower energy position as compared to the band energy absorption as showed in Figure 68. From the fundamental point of view, a wide variety of semiconductor can be expected to generate tunable dopant emission in different spectral window once they get successfully doped with Mn and Cu. Either Mn or Cu substitute Zn ions in ZnS crystals introducing a trap energy level, where electron and hole can be trapped. An electron can undergo photo-excitation process

in the host ZnS lattice of nanoparticles and consequently decay via a non-radiative transition from the $^4T_1$ level to the $^6A_1$ level [231]. The strong emission could be attributed to the radiative decay between those localized states of Mn and Cu inside the ZnS band gap. This particular type of materials can be utilized as fluorescent materials in OLED displays.
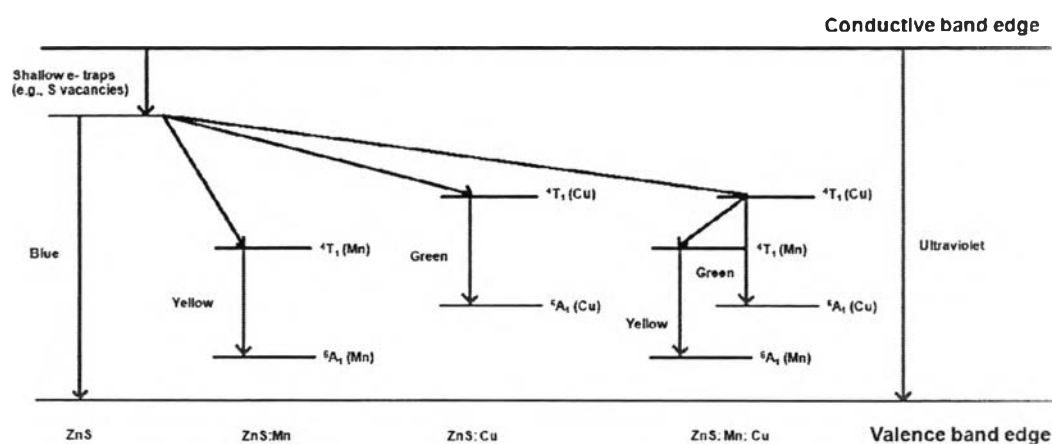

Figure 10.6 Energy level of ZnS, Mn-doped ZnS and Cu-doped ZnS

10.5 Conclusion

ZnS and metal (Mn, Cu)-doped-ZnS were successfully synthesized via wet chemical synthetic method. FTIR and X-ray diffraction can be used to identify the chemical bonding and crystal structure. The metals (Mn, Cu) can be completely substituted to ZnS lattice. SEM revealed that their particle was blocky particle with irregular sharp. The laser confocal microscope and photoluminescence spectroscopy showed that as-synthesized ZnS and metal (Mn, Cu)-doped-ZnS exhibited light emission. The photophysical insights were studied. ZnS emits light tunable in the entire visible window by incorporating Mn and Cu dopant, suggesting that the luminescent centers were transferred to impurity ions.

10.6 Acknowledgement

10.7 References

J.M. Hwang, et al., Preparation and characterization of ZnS based nanocrystalline particles for polymer light-emitting diodes, Current Applied Physics 5 (1) (2005) 31e34.

H. Cho, et al., Highly flexible organic light-emitting diodes based on ZnS/Ag/ WO3 multilayers transparent electrodes, Organic Electronics 10 (6) (2009) 1163e1169.

C.W. Lee, et al., Investigations of organic light emitting diodes with CdSe (ZnS) quantum dots, Materials Science and Engineering: B 147 (2e3) (2008) 307e311.

X. Liu, et al., ZnS/Ag/ZnS nano-multilayer films for transparent electrodes in flat display application, Applied Surface Science 183 (1e2) (2001) 103e110.

V. Dimitrova, J. Tate, Synthesis and characterization of some ZnS-based thin film phosphors for electroluminescent device applications, Thin Solid Films 365 (1) (2000) 134e138.

D.W. Wang, et al., The improvement of near-ultraviolet electroluminescence of ZnO nanorods/MEH-PPV heterostructure by using a ZnS buffer layer, Organic Electronics 12 (1) (2011) 92e97.

E.A. Mastio, et al., The effects of multiple KrF laser irradiations on the electroluminescence and photoluminescence of rf-sputtered ZnS: Mn-based electroluminescent thin film devices, Applied Surface Science 157 (1e2) (2000) 74e80.

B.L. Zhu, et al., Fabrication of ZnS semiconductor nanodisks in layered organicinorganic solid templates, Thin Solid Films 474 (2005) 114e118.

C. Ma, et al., Nanobelts, Nanocombs, and nano-windmills of wurtzite ZnS, Advanced Materials 15 (2003) 228e231.

Y. Zhao, et al., Low temperature synthesis of hegagonal (Wurtzite) ZnS nanocrystals, Journal of the American Ceramic Society 126 (2004) 6874e6875.

B. Dong, et al., Synthesis and characterization of the water-soluble silicacoated ZnS: Mn nanoparticles as fluorescent sensor for Cu2□ ions, Journal of Colloid and Interface Science 339 (1) (2009) 78e82.

N. Uzar, S. Okur, M.C. Arikan, Investigation of humidity sensing properties of ZnS nanowires synthesized by vapor liquid solid (VLS) technique, Sensors and Actuators A: Physical 167 (2) (2011) 188e193.

L. Luo, et al., A cataluminescence gas sensor for carbon tetrachloride based on nanosized ZnS, Analytica Chimica Acta 635 (2) (2009) 183e187.

M. Geszhe, et al., Folic acid-conjugated core/shell ZnS: Mn/ZnS quantum dots as targeted probes for two photon fluorescence imaging of cancer cells, Acta Biomaterialia 7 (3) (2011) 1327e1338.

X. Jiang, et al., Simultaneous in situ formation of ZnS nanowires in a liquid crystal template by ç-irradiation, Chemistry of Materials 13 (2001)

1213e1218.

T. Charinpanitkul, et al., Effect of cosurfactant on ZnS nanoparticle synthesis in microemulsion, Science and Technology of Advanced Materials 6 (2005) 266e271.

Y. Li, et al., Synthesis of ZnS nanoparticles into the pore of mesoporous silica spheres, Materials Letters 63 (2009) 1068e1070.

M. Salavati-Niasari, M.Z. Loghman-Estarki, F. Davar, Controllable synthesis of wurtzite ZnS nanorods through simple hydrothermal method in the presence of thioglycolic acid, Journal of Alloys and Compounds 475 (2009) 782e788.

N. Uekawa, et al., Synthesis of stable sol of ZnS nanoparticles by heating the mixture of ZnS precipitate and ethylene glycol, Colloids and Surfaces A: Physicochemical and Engineering Aspects 361 (2010) 132e137.

B.S. Rema Devi, R. Raveendran, A.V. Vaidyan, Synthesis and characterization of Mn2$\square$-doped ZnS nanoparticles, Pramana Journal of Physics 68 (2007) 679.

M. Kuppayee, G.K. Vanathi Nachiyar, V. Ramasamy, Synthesis and characterization of Cu2 $\square$ doped ZnS nanoparticles Applied Surface Science 257 (2011) 6779e6786.

K. Nakamoto, Infrared and Raman Spectra of Inorganic and Coordination Compounds, 5 ed. John Wiley, New York, 1997.

S.B. Qadri, et al., Size-induced transition-temperature reduction in nanoparticles of ZnS, Physical Review B 44 (1999) 153.

H. Hu, W. Zhang, Synthesis and properties of transition metals and rare earth

metals doped ZnS nanoparticles, Optical Materials 28 (2006) 36e50.

H. Teruhiko, K. Hiroji, Luminescence excitation spectra and their exciton strucutres of ZnS phosphors. I. Mn, (Cu, Al), and (Au, Al) doped phosphors, Japanese Journal of Applied Physics 19 (2) (1980) 267.

R.N. Bhargava, D. Gallagher, Optical properties of manganese-doped nanocrystals of ZnS, Physics Review Letters 72 (1994) 416e419